Rodríguez Pérez, AM.; Selga, J.; Sans, M.; Martin, F.; Boria Esbert, VE. (2017). Automated design of bandpass filters based on open complementary split ring resonators (OCSRRs) using aggressive space mapping (ASM) optimization. International Journal of Numerical Modelling Electronic Networks Devices and Fields. 30(3-4):1-11. https://doi.org/10.1002/jnm.2121

Automated Design of Bandpass Filters based on Open Complementary Split Ring Resonators (OCSRRs) using Aggressive Space Mapping (ASM) Optimization

[1]Ana Rodríguez, [2]Jordi Selga, [2]Marc Sans, [2]Ferran Martín, [1]Vicente Boria

[1]Departamento de Comunicaciones-iTEAM, Universitat Politècnica de València, 46022 Valencia, Spain. E-mail: vboria@dcom.upv.es

[2]GEMMA/CIMITEC, Departament d'Enginyeria Electrònica, Universitat Autònoma de Barcelona, 08193 Bellaterra, Spain. E-mail: Ferran.Martin@uab.es

Abstract

This paper is focused on the design of bandpass filters based on open complementary split ring resonators (OCSRRs) in microstrip technology. The filters are obtained by coupling the corresponding shunt resonators (OCSRRs) through admittance inverters (quarter wavelength transmission line sections). Different undesirable effects derived from the chosen topology are taken into account and are compensated at the design level. These effects include the reduction in bandwidth (caused by the narrowband functionality of the line sections acting as admittance inverters), and the presence of a spurious band above the filter pass-band. The proposed technique is based on the well-known aggressive space mapping (ASM) algorithm, which is a powerful tool for the synthesis and design of microwave components. The design of the OCSRR-based filter is provided in a fully automated way as the main result of this paper.

Keywords: space mapping, OCSSRs, artificial transmission lines, bandpass filters, microstrip technology.

1. Introduction

Bandpass filters are present in numerous RF/microwave applications (communications, radar or measurement systems). The design of conventional filters, as it is widely reported in the literature [1], is commonly done by applying network synthesis methods, combined with the use of full-wave electromagnetic (EM) solvers (due to the lack of accuracy of the circuit models). However, the classical design approach (network synthesis) is not valid for the case of wideband filters, due to the narrowband behavior of the real inverters that yields to a bandwidth reduction in practice. Having this in mind, an automated strategy that overcomes that effect by adding a previous stage is proposed. It consists in calculating the lumped element values of a filter that allows its corresponding schematic to satisfy the wanted specifications, see Section 4. Starting from the electrical performance of the filter defined in terms of fractional bandwidth (*FBW*), in-band ripple

level (L_{ar}), center frequency (f_0), and filter order (n), the final dimensions of the filter geometry are determined.

The filters synthesized in this work are implemented in microstrip technology using open complementary split ring resonators (OCSRRs) coupled through admittance inverters (in practice quarter-wavelength transmission lines), see Fig. 1. OCSRRs are a particular type of electrically small planar resonators [2-3]. By loading a microstrip line with shunt connected OCSRR an LC tank behavior with an additional transmission zero is achieved (see Fig. 2). This is a very interesting property for filter applications in order to increase the selectivity of the filter, see more details in Section 2.

The present contribution is an improvement of a preliminary work [4]. Both works synthesize the same type of bandpass filters and use space mapping (SM) algorithms [5-6] to determine the OCSRR unit cell layout. SM algorithms are a set of techniques that provide a smart way to automate microwave design by typically combining the accuracy of a fine model (typically an EM field simulation) with the speed of a coarse model (e.g. equivalent circuit model). This allows to obtain the optimal design, without a direct optimization of the fine model and hence improving the efficiency.

In this paper, a more accurate design approach, with respect to that one used in [4], is proposed. It uses a two-step algorithm, similarly to the one recently published in [7], where stepped impedance resonators (SIRs) and grounded stubs were used instead of OCSRRs. The first optimization stage finds the optimal schematic that satisfies the requested specifications (taking into account the narrow band functionality derived from the use of inverters based on real transmission lines), while the second determines the final dimensions of the different involved resonators. Furthermore, in this contribution, the undesired spurious band that is present in this type of filters, located at $2f_0$ (being f_0 the central frequency of the filter), is suppressed (see references [4], [8-9]). The method is validated with two different examples. For the first example, a bandpass filter of order n=3, was designed, manufactured and measured. In the second example a filter of higher order (n=5) was simulated and compared with the optimal circuit response to show the validity and potentiality of this methodology.

2. Topology of the proposed bandpass filters based on OCSRRs

The filters synthesized in this work are based on shunt resonators (equivalent circuit model of OCSRRs) coupled through admittance inverters. The general configuration of a bandpass filter using admittance inverters is shown in Fig. 1.a, as reported in [1]. The inverters are implemented by transmission lines sections with 90^0 phase shift at f_0.

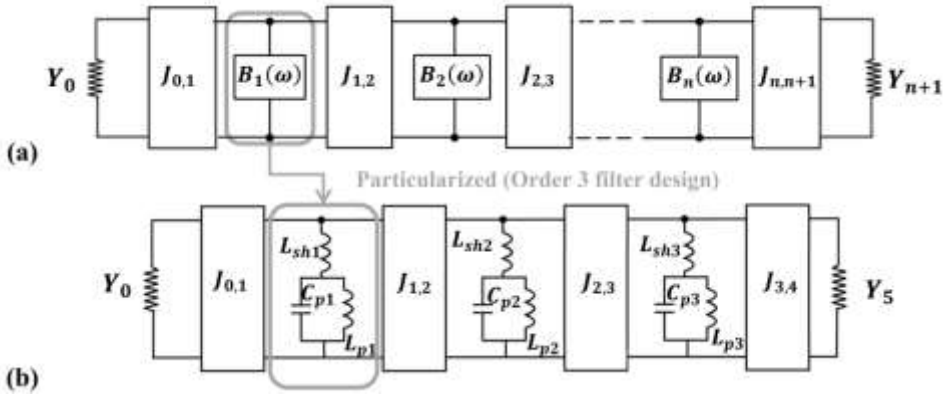

Fig 1. - Generalized bandpass filter network (a). Particularized design for the filter implemented with OCSRRs of order *n*=3 (b).

In the case of considering identical admittance inverters, *i.e.* $J_{0,1}=\ldots=J_{n,n+1}=J$, the susceptance slope parameter (b_i) of each cascaded section *i* can be directly calculated, using the following expressions [1]:

$$b_1 = \frac{{J_{0,1}}^2\ \Omega_c\ g_0 g_1}{Y_0\ FBW} \tag{1}$$

$$b_{i+1} = \frac{{J_{i,i+1}}^2\ {\Omega_c}^2\ g_i\ g_{i+1}}{b_i\ FBW^2} \tag{2}$$

$$b_n = \frac{{J_{n,n+1}}^2\ \Omega_c\ g_n g_{n+1}}{Y_{n+1}\ FBW} \tag{3}$$

being g_i the element values of a Chebyshev lowpass prototype filter of order *n*, which presents a passband ripple of L_{ar} dB, a fractional bandwidth *FBW* and cutoff frequency Ω_c. The terms Y_0 and Y_{n+1} correspond to the input and output impedance respectively, and in that topology are set equal to the characteristic admittance of the quarter-wavelength transmission lines that act as inverters.

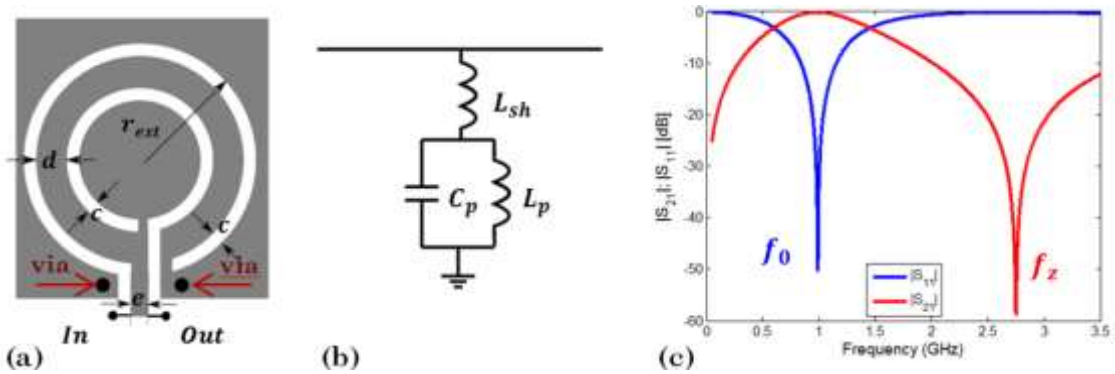

Fig 2. - OCSRR shunt connected to microstrip line. Unit cell layout (a), equivalent circuit (b), and frequency response of S-parameters magnitude (c).

The equivalent circuit model corresponding to a shunt-connected OCSRR in a microstrip line is illustrated in Fig. 2.b and also in Fig. 1.b (where the general topology of each resonator has been replaced with the one of an OCSRR). Basically, the OCSRR

is modeled by the LC tank of inductance and capacitance L_p and C_p, respectively, while L_{sh} models the presence of the strip between the inner metallic region of the OCSRR and the signal strip of the host line where the ports are attached (denoted as In and Out in the layout depicted in Fig. 2.a). This cell, as graphically illustrated in Fig. 2.c, exhibits a passband response followed by a stop-band. Two different frequencies can be clearly identified: the one at which the transmission zero appears (f_z), and the reflection zero frequency (f_0). Therefore, the value of the f_z can be easily derived from the circuital model (Fig. 2.b), as the one that makes the shunt impedance to be zero:

$$\omega_z = 2\pi f_z = \sqrt{\frac{1}{C_p} \cdot \left(\frac{1}{L_p} + \frac{1}{L_{sh}}\right)} \tag{4}$$

while the reflection zero appears when the shunt admittance is equal to zero:

$$\omega_0 = 2\pi f_0 = \frac{1}{\sqrt{L_p C_p}} \tag{5}$$

The resulting susceptance of the resonator considered can be also calculated as:

$$B = \frac{\omega^2 L_p C_p - 1}{\omega\left(L_{sh} L_p C_p \omega^2 - L_{sh} - L_p\right)} \tag{6}$$

The slope parameter b is defined for every filter section i (see [1]) as:

$$b_i = \frac{\omega_0}{2} \frac{dB_i}{d\omega}\bigg|_{\omega=\omega_0} \tag{7}$$

being ω_0 the angular central frequency of the filter. So, the slope parameter inferred for this type of resonator is equal to $\left(1/\omega_0 L_{p_i}\right)$. Hence, the equivalent lumped element values can be obtained straight forward from the angular frequencies ω_z and ω_0 defined in (4)-(5), and the corresponding values b_i previously calculated with equations (1)-(3), applying the following expressions:

$$L_{p_i} = \frac{1}{\omega_0 b_i} \tag{8}$$

$$C_{p_i} = \frac{1}{{\omega_0}^2 L_{p_i}} = \frac{b_i}{\omega_0} \tag{9}$$

$$L_{sh_i} = \frac{L_{p_i}}{{\omega_z}^2 - {\omega_0}^2} \cdot {\omega_0}^2 = \frac{\omega_0}{b_i \cdot ({\omega_z}^2 - {\omega_0}^2)} \tag{10}$$

All the resonators must be designed to have the same transmission zero (f_z); otherwise a spurious band may appear above the passband. Usually this value is considered to be $2f_0$, since it is where the unwanted passband commonly appears in this kind of structures due to the non-ideality of the inverters. This issue was not considered in previous works

[4, 9], and it is relevant for obtaining a better filter performance. The typical topology and circuit schematic of the considered bandpass filter are depicted in Fig. 3.

Let us consider as case of study the filter with the specifications summarized in Table 1. The circuital values obtained for this filter considering equal line sections of characteristic admittance $J_{i,i+1}$ = 0.02 S (50 ohms), are summarized in Table 2, and the frequency response is represented with a black solid line in Fig. 4.

Table 1.- Filter specifications

	L_{ar}	*FBW*	Central frequency f_o	Order(*n*)
Chebyshev Filter	0.01dB	23%	2GHz	3

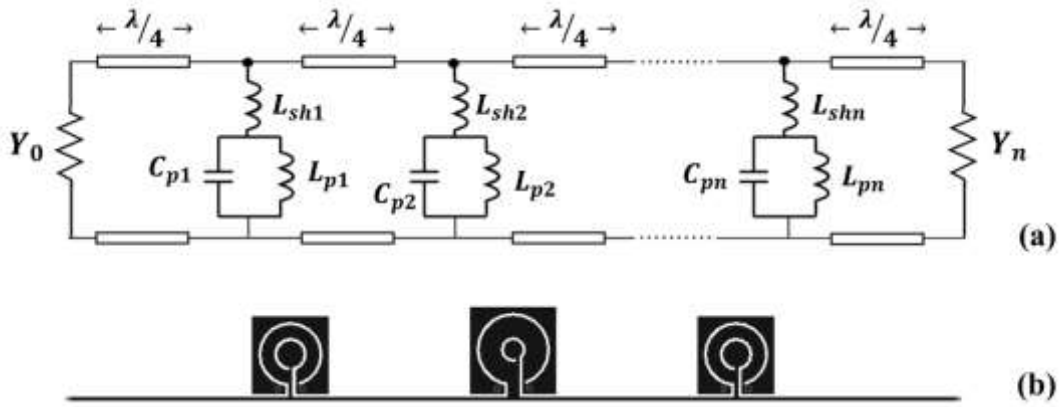

Fig 3. - Schematic of the proposed bandpass filters (a). Typical topology for an order-3 filters (b).

If ideal inverters (see Fig. 3.a) are replaced by 50-Ω quarter wavelength transmission line sections at the central frequency f_0, the filter does not meet the specifications. This is due to the limited functionality of these transmission lines as admittance inverters (just valid in a narrow band range). In order to achieve a filter response closer to the ideal one, an optimization at the schematic level should be performed (see Section 4), before proceeding to find the resonator dimensions.

Table 2.- Values obtained for the filter specifications of Table 1 (f_z[GHz]=4, $J_{i,i+1}[S]\big|_{i=0\text{ to }3}$=0.02)

	L_{pi} [nH]	C_{pi} [pF]	L_{shi}[nH]
Resonators *i*=1, 3	1.4545	4.3539	0.5190
Resonator *i*=2	0.9432	6.7142	0.3365

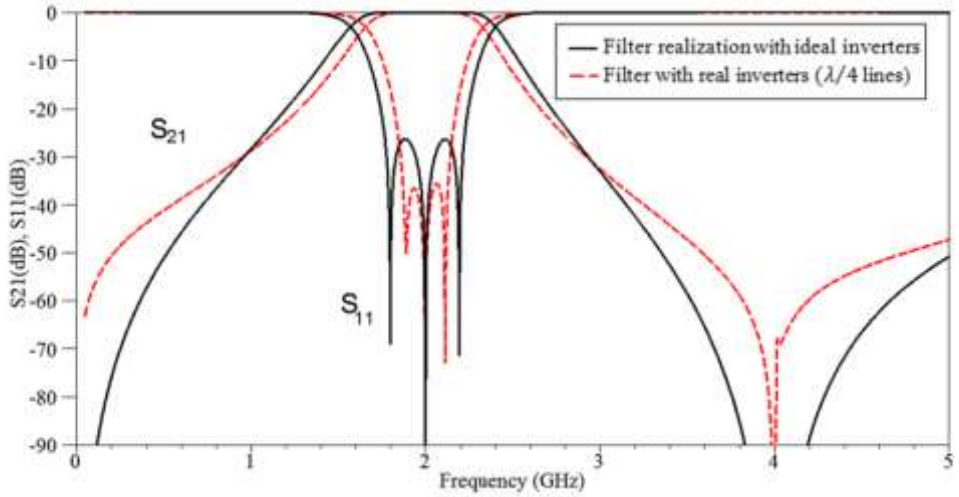

Fig 4. - Comparison between the scattering parameters response (in magnitude) of: the ideal schematic of Chebyshev model (Fig. 1.b), and the ideal schematic where the inverters are replaced with quarter-wavelength transmission lines (Fig. 3.a)

3. General formulation of aggressive space mapping (ASM)

The methodology proposed in Section 4 for the synthesis of the considered filters is based on aggressive space mapping (ASM) [10], and hence the general formulation is given next for completeness. It is assumed that for any optimization based on space mapping, there are two different models that can describe the same physical system/structure. An expensive model of primary interest (known as fine model), and a cheaper (denoted coarse model) which is less accurate but much faster. The key idea is to find the transformation *P* which relates the parameters of the fine model (vector $\mathbf{x_f}$) with the parameters of the coarse model (vector $\mathbf{x_c}$):

$$\mathbf{x_c} = \mathbf{P}(\mathbf{x_f}) \tag{11}$$

such that the responses of the two models ($\mathbf{R_c}$ and $\mathbf{R_f}$) are equal in the region of interest:

$$\mathbf{R_c}\big(\mathbf{P}(\mathbf{x_f})\big) \approx \mathbf{R_f}(\mathbf{x_f}) \tag{12}$$

In the case of EM applications, the magnitude of a transfer function at certain frequency range (e.g. $|S_{21}|$) is usually chosen as responses. Focusing on the considered approach, called ASM, the solution is found iteratively by solving the following non-linear system:

$$\mathbf{f}(\mathbf{x_f}) = 0 \tag{13}$$

where

$$\mathbf{f}(\mathbf{x_f}) = \mathbf{P}(\mathbf{x_f}) - \mathbf{x_c^*} \tag{14}$$

being $\boldsymbol{x_c}^*$ the target coarse model vector. Let us assume that $\mathbf{x_f}^{(j)}$ is the solution of (13) at the *j*-th iteration. The next iterate $\mathbf{x_f}^{(j+1)}$ is found by applying a quasi-newton step $\mathbf{h}^{(j)}$:

$$\mathbf{x_f}^{(j+1)} = \mathbf{x_f}^{(j)} + \mathbf{h}^{(j)} \tag{15}$$

where $\mathbf{h^{(j)}}$ is calculated according to:

$$\mathbf{B}^{(j)} \cdot \mathbf{h}^{(j)} = -\mathbf{f}\left(\mathbf{x_f}^{(j)}\right) = -\mathbf{f}^{(j)} \tag{16}$$

and being $\mathbf{B^{(j)}}$ the mapping matrix, which is an approximation of the Jacobian matrix of the vector **f** with respect to $\mathbf{x_f}$ at the *j*-th iteration. At each iteration, this mapping matrix is updated according to the expression:

$$\mathbf{B}^{(j+1)} = \mathbf{B}^{(j)} + \frac{\mathbf{f}^{(j+1)}\mathbf{h}^{(j)^T}}{\mathbf{h}^{(j)^T}\mathbf{h}^{(j)}} \tag{17}$$

where the super-index *T* stands for transpose. The algorithm iterates till the error of the norm of the error function *f* defined in (14) is smaller than a fixed small positive constant η ($\eta \rightarrow 0$), or the maximum number of iterations of the algorithm N_{max} is reached.

4. The automated synthesis method

The optimization is performed in two different stages. At the first stage, the target circuital parameters values from the circuital model of Fig. 3.a) are determined. These parameters provide a response that satisfies the target specifications in a good approximation. Next, with the second ASM based optimization, a practical physical solution is found, i.e. the geometrical dimensions of the different resonators are calculated.

4.1.First stage: determination of the optimal schematic

Following the terminology of space mapping, the coarse model for this first ASM is the generalized bandpass filter network based on shunt resonators coupled through "ideal" admittance inverters. The equations which describe univocally this coarse model are the classical formulas of a Chebyshev filter using admittance inverters and shunt LC resonators. The coarse model vector $\mathbf{x_c}$ is composed then by the set of specifications of the Chebyshev filter: f_{o_c}, FBW_c and L_{ar_c}, which brings the ideal Chebyshev response. It is worth mentioning, that the transmission zero frequencies originated by the OCSRRs are fixed to $f_z=2f_0$ (a different value could be chosen, but once fixed it will remain constant, i.e. it will not be considered an optimization parameter by itself).

On the other hand, the optimal schematic (used as fine model) is obtained substituting the ideal inverters by real transmission lines (quarter wavelength) and the ideal shunt resonators with the equivalent circuit of the OCSRRs as shown in Fig. 3.a. The vector ($\mathbf{x_f}$) that defines that model, has a similar set of parameters: f_{o_f}, FBW_f , L_{ar_f}. The target specifications of the filter are the ones given for the ideal Chebyshev filter: $\mathbf{x_c}^* = [f_{o\_c}^*, FBW_c^*, L_{ar\_c}^*]$. The lumped parameters which define each resonator *i* (L_{pi}, C_{pi} and L_{shi}) are automatically obtained from the new set of performance parameters (f_0, *FBW* and L_{ar}) found with the ASM-based algorithm.

According to the general flowchart of ASM, the first step is to infer the initial point $\mathbf{x_f^{(1)}}$, that in this case is assumed to be $\mathbf{x_f}^{(1)} = \mathbf{x_c}^*$, since the same type of parameters are considered for both spaces. By evaluating $\mathbf{x_f}^{(1)}$ (i.e. schematic simulation) it is also easy to obtain $\mathbf{x_c^{(1)}}$ by parameter extraction, and as result the error function is evaluated for the first iteration using expression (14). Next issue is the initialization of the mapping matrix, calculated according to:

$$\mathbf{B^{(1)}} = \begin{pmatrix} \frac{\delta FBW_c}{\delta FBW_f} & \frac{\delta FBW_c}{\delta L_{ar\_f}} & \frac{\delta FBW_c}{\delta f_{0\_f}} \\ \frac{\delta L_{ar\_c}}{\delta FBW_f} & \frac{\delta L_{ar\_c}}{\delta L_{ar\_f}} & \frac{\delta L_{ar\_c}}{\delta f_{0\_f}} \\ \frac{\delta f_{0\_c}}{\delta FBW_f} & \frac{\delta f_{0\_c}}{\delta L_{ar\_f}} & \frac{\delta f_{0\_c}}{\delta f_{0\_f}} \end{pmatrix} \tag{18}$$

The initial matrix is obtained after applying the perturbation constants over each of the considered parameters. Afterwards, the normal evolution of the ASM algorithm is followed, till the algorithm finishes, i.e. when the norm given by:

$$\left\|\mathbf{f_{norm}}^{(j)}\right\| = \sqrt{\left(1 - \frac{f_{0\_c}^{(j)}}{f_{0\_c}{}^*}\right)^2 + \left(1 - \frac{FBW_c^{(j)}}{FBW_c^*}\right)^2 + \left(1 - \frac{L_{Ar\_c}^{(j)}}{L_{Ar\_c}{}^*}\right)^2} \tag{19}$$

is sufficiently small or the maximum number of iterations is achieved. At the end of this process, the optimal filter schematic is obtained: L_{pi}, C_{pi} and L_{shi}. Note that the optimal schematic is just a rough approximation of the ideal Chebyshev filter and that we have called quasi-Chebyshev filter. For instance, the position of the reflection zeros frequencies is not the same in both responses. The reason is that these frequency positions are not goals in the optimization process, and the optimization is done trying to preserve the requested fractional bandwidth.

4.2.Second stage: layout determination (OCSRRs)

In the second ASM-optimization, the fine model is the physical model (EM-model) of the OCSRR depicted in Fig. 2.a, while the coarse model is given by its equivalent circuit of Fig. 2.b, whose values are found in the previous stage. The same numbers of parameters are considered in both spaces (i.e. validation and optimization spaces) because the mapping matrix **B** of the ASM algorithm needs to be inverted, and in such a case we prevent the algorithm from potential instabilities. Only three of the geometrical dimensions are chosen as design variables, and the other ones are either expressed as a function of the previous ones or taken as constant values (in this case *c* is fixed to 0.20mm and the via diameter to 0.4mm). The circuit parameters that electrically model the resonator constitute the coarse vector: $\mathbf{x_c} = [L_p, C_p, L_{sh}]$. On the other hand, the fine model is described by the radius of the outer open-ring (r_{ext}), the distance between the slots of width *c* (i.e. *d*), and the width of the inner strip that opens the outer ring (*e*), $\mathbf{x_f} = [r_{ext}, d, e]$. The initial layout $\mathbf{x_f^{(1)}}$ is inferred from the target vector $\mathbf{x_c}^*$ by means of analytical

formulas [11-12] which relate the electrical parameters and the geometrical dimensions. The final layout is obtained when the normalized error function, given by:

$$\left\|\mathbf{f}_{\mathbf{norm}}{}^{(j)}\right\| = \sqrt{\left(1-\frac{L_p^{(j)}}{L_p^*}\right)^2+\left(1-\frac{C_p^{(j)}}{C_p^*}\right)^2+\left(1-\frac{L_{sh}^{(j)}}{L_{sh}^*}\right)^2} \qquad (20)$$

is considered sufficiently small (<2%). The mapping matrix **B** is initialized by slightly perturbing OCSRR dimensions (r_{ext}, d and e) and obtaining the values of C_p, L_p and L_{sh} from parameter extraction. More details about this second algorithm can be found in [4].

5. Design examples

Two different examples are shown to illustrate and validate the method: order 3 and order 5 bandpass filters. The first example has been also manufactured and measured. The considered substrate is the commercial Rogers RO3010 with thickness h= 0.254mm and dielectric constant ε_r =10.2. Even though it is not possible to perfectly match the Chebyshev (target) response by replacing the ideal admittance inverters with transmission line sections, it is possible to find a very good approximation.

5.1. Order-3 Filter

Applying the first developed ASM algorithm to the example of Table 1, the corresponding fine parameters are inferred (see Table 3). Only four iterations are needed for their determination.

Table 3.- Over-dimensioned filter specifications (output of first ASM)

L_{ar_f} [dB]	FBW_f	f_{o_f} [GHz]
0.0267	36.79%	2.0571

The circuit element values that define the optimal filter schematic (individual OCSRRs) are shown in Table 4. The agreement in terms of central frequency and bandwidth is good, as it is graphically illustrated in Fig. 5 (compare the circuital schematic responses corresponding to grey and blue dotted lines traces).

Table 4.- Electrical parameters for the optimal filter schematic (Fig. 3.a)

	L_{pi} [nH]	C_{pi} [pF]	L_{shi}[nH]
Resonators *i*=1, 3	1.8529	3.2305	0.6176
Resonator *i*=2	1.3363	4.4794	0.4454

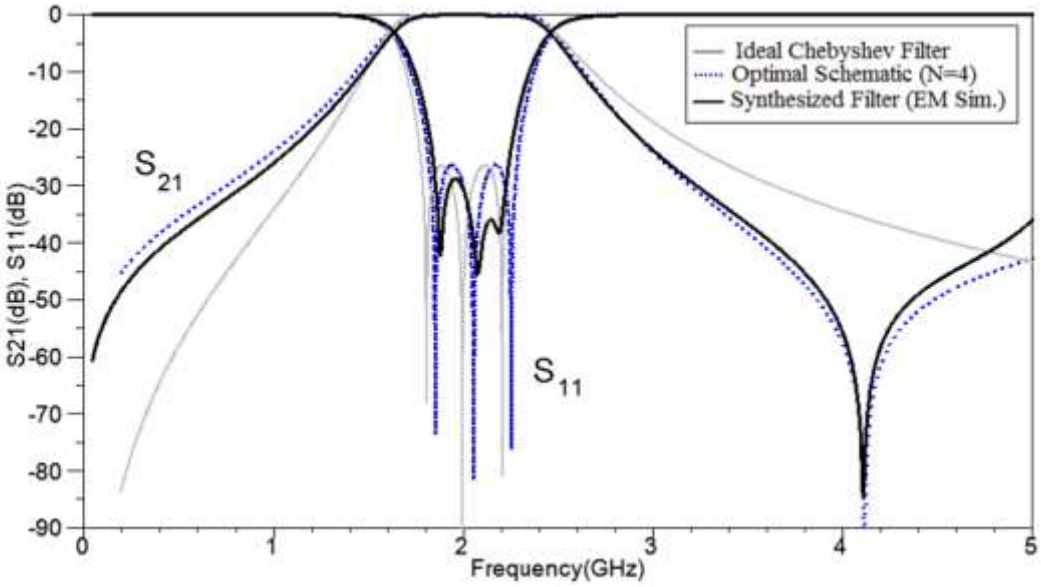

Fig 5.- Frequency response of the designed bandpass filter: EM simulation (black solid line), circuital simulation of ideal Chebyshev filter (grey line), and optimal-schematic (blue dotted line).

Using the ASM-based synthesis tool, the dimensions of the OCSRRs are determined as it is summarized in Table 5 and Table 6. The width of the slot rings (*c*) was fixed to 0.2mm. It is worth mentioning that the total effort in terms of full-wave EM simulations, is 12 (9 iterations of the ASM algorithm, plus 3 EM corresponding to the mapping matrix initialization $\mathbf{B}^{(1)}$).

Table 5.- Fine parameters for the initial and final layout, number of iteration needed and errors

Resonator 1,3	r_{ext}**[mm]**	***d*[mm]**	***e*[mm]**	**It. No**	$\left\|\mathbf{f}_{norm}^{(j)}\right\|$	f_0**[GHz]**	f_z**[GHz]**
Initial layout	3.450	1.399	0.270	1	2.0764	0.928	2.085
Final layout	2.123	0.860	0.338	9	0.0163	2.058	4.136

Table 6.- Fine parameters for the initial and final layout, number of iterations needed and errors

Resonator 2	r_{ext}**[mm]**	***d*[mm]**	***e*[mm]**	**It. No**	$\left\|\mathbf{f}_{norm}^{(j)}\right\|$	f_0**[GHz]**	f_z**[GHz]**
Initial layout	3.50	0.862	0.483	1	2.2023	0.819	2.167
Final layout	2.419	1.445	0.944	7	0.0071	2.062	4.114

The magnitude response of the scattering parameters of the central resonator (i = 2) is depicted in Fig. 6 (circuital and electromagnetic responses), giving an error under 1% according to Table 6.

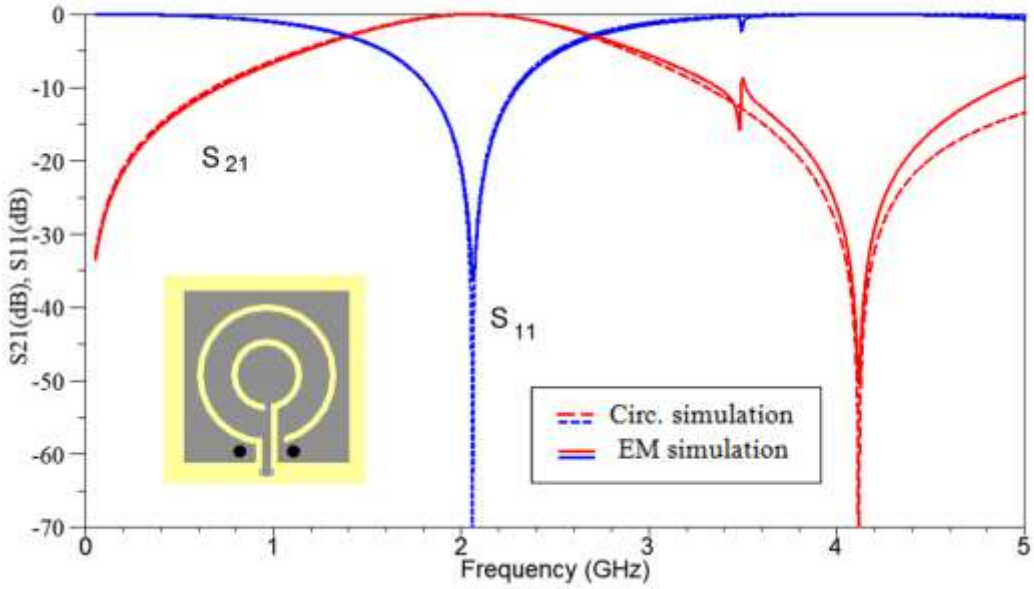

Fig 6.- Frequency response of the central resonator (*i*=2): circuital simulation(dashed line) and the EM response of the found synthesis (solid line). Layout of the resonator is also shown.

Once each resonator cell has been synthesized, the cells are simply cascaded with the transmission line sections in order to generate the final filter layout. The length of the transmission line sections (to implement the inverters) is obtained automatically by a line calculator (provided by the software), which can be considered a quite good approximation. The dimensions provided by the Ansys Designer for a 50 Ω line (electrical length of 90º) for the considered substrate (Rogers RO3010) at the frequency of interest f_{o_f} are: length l = 14.705mm and width w = 0.221mm. It is expected that the presence of the resonator can add some extra phase shift that was not initially considered (i.e. electrical length slightly different of 90º at the central frequency), and can have some effect in the in-band return loss lobe levels. To minimize that effect, an optimization of the line width should be performed to present a 90 degrees electrical length at the central frequency of the filter (as considered in the order-5 filter example). In Fig. 7, it is represented the lossless electromagnetic response of the filter (red dashed line) which is very close to the target response given by the optimized schematic (blue dotted line), and also to the Chebyshev target (grey solid trace). The agreement between the target (schematic) response and the electromagnetic simulation of the synthesized layout (losses are not included) is in reasonable agreement. Since the unit cells are already sufficiently spaced, coupling effects are not observed.

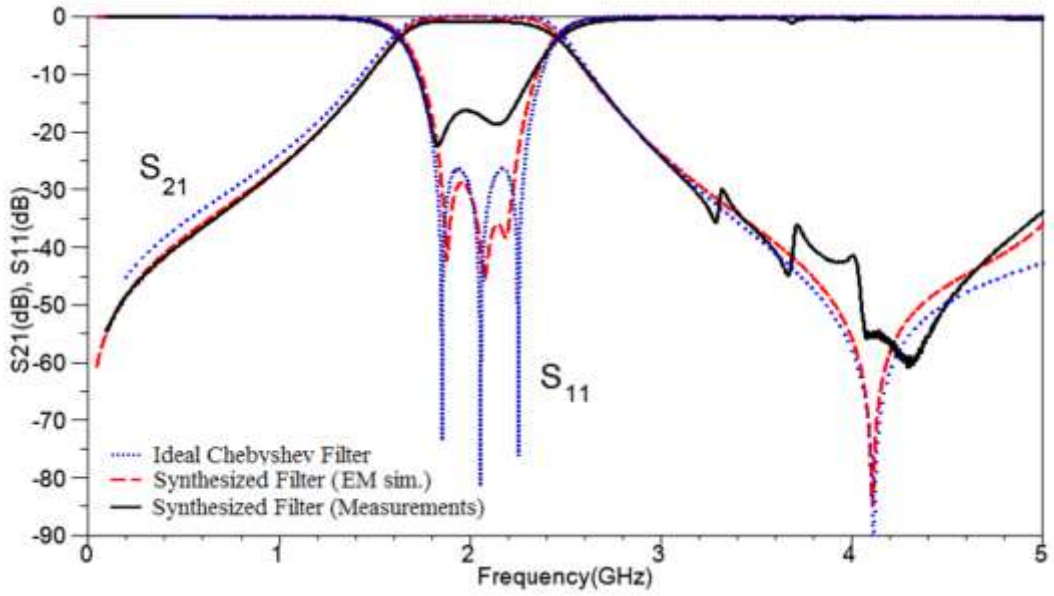

Fig 7.- Comparison between the frequency response of the manufactured filter (solid black line), optimal-schematic (blue dotted line) and EM lossless response (red dashed line).

The filter was fabricated with an LPKF ProtoMat HF-100 drilling machine, being the layout depicted in Fig. 8. The measured response illustrated in Fig. 7 is also in reasonable agreement with the full-wave EM simulation data. Obviously there are differences between simulation and measurements, but using "in-house" manufacturing technology, together with the employed thin substrate (0.254mm), it is very difficult to preserve the exact location and number of reflection zeros, as well as the frequency value for the achieved transmission zero.

Fig 8.- Photograph of the manufactured filter.

5.2.Order-5 Filter

The second filter example is a filter of higher order bandwidth, described by the specifications of Table 7. In this case the dimensions of three different resonators have to be determined.

Table 7.- Filter specifications

	L_{ar}	*FBW*	Central frequency (f_o)	Order(n)
Chebyshev Filter	**0.05dB**	**42%**	**2GHz**	**5**

The optimal filter specifications, meaning the fine parameters for the optimal schematic filter, are summarized in Table 8. The first ASM algorithm converged in just 5 iterations.

Table 8.- Over-dimensioned filter specifications (output of first ASM)

L_{ar_f} [dB]	FBW_f	f_{o_f} [GHz]
0.6699	0.0796	2.072

The circuit element values that correspond to the calculated optimal filter schematic (individual OCSRRs) are shown in Table 9.

Table 9.- Electrical parameters for the target filter schematic

	L_{pi}[nH]	C_{pi} [pF]	L_{shi}[nH]
Resonators *i*=1,5	2.3512	2.5077	0.7837
Resonators *i*=2,4	1.8701	3.1527	0.6234
Resonator *i*=3	1.3376	4.4078	0.4459

Following the same design strategy explained before, the dimensions for the different resonators are calculated by applying ASM to the different resonators, yielding to the layout of the filter illustrated in Fig. 9. In this case, the transmission line sections are calculated for presenting a 50 Ω behavior at the central frequency with the planar EM solver optimizer (just the width of the line). The values obtained for the different resonators are summarized in tables 10-12. As in the previous example, note that the table shows the number of iterations of ASM-simulation, but the cost in evaluations of the fine model is the number of iterations plus three (which is the number of simulations that are needed to estimate the initial mapping matrix $\mathbf{B}^{(1)}$).

Fig 9.-Layout of the synthesized 5-order filter (top).

Table 10.- Fine parameters for the initial and final layout, number of iterations needed and errors

Resonators 1,5	r_{ext}[mm]	*d*[mm]	*e*[mm]	It. No	$\|\mathbf{f}_{norm}^{(j)}\|$	f_0[GHz]	f_z[GHz]
Initial Layout	3.250	0.940	0.250	1	2.3957	0.980	2.199
Final Layout	1.841	0.511	0.121	7	0.0147	2.077	4.156

Table 11.- Fine parameters for the initial and final layout, number of iterations needed and errors

Resonators 2,4	r_{ext}[mm]	*d*[mm]	*e*[mm]	It. No	$\|\mathbf{f}_{norm}^{(j)}\|$	f_0[GHz]	f_z[GHz]
Initial Layout	3.250	1.089	0.265	1	2.188	0.930	2.046
Final Layout	2.094	0.828	0.316	8	0.0067	2.074	4.150

Table 12.- Fine parameters for the initial and final layout, number of iterations needed and errors

Resonator 3	r_{ext}[mm]	*d*[mm]	*e*[mm]	It. No	$\|\mathbf{f}_{norm}^{(j)}\|$	f_0[GHz]	f_z[GHz]
Initial Layout	3.250	1.089	0.265	1	2.188	0.930	2.046
Final Layout	2.094	0.828	0.316	8	0.0067	2.074	4.150

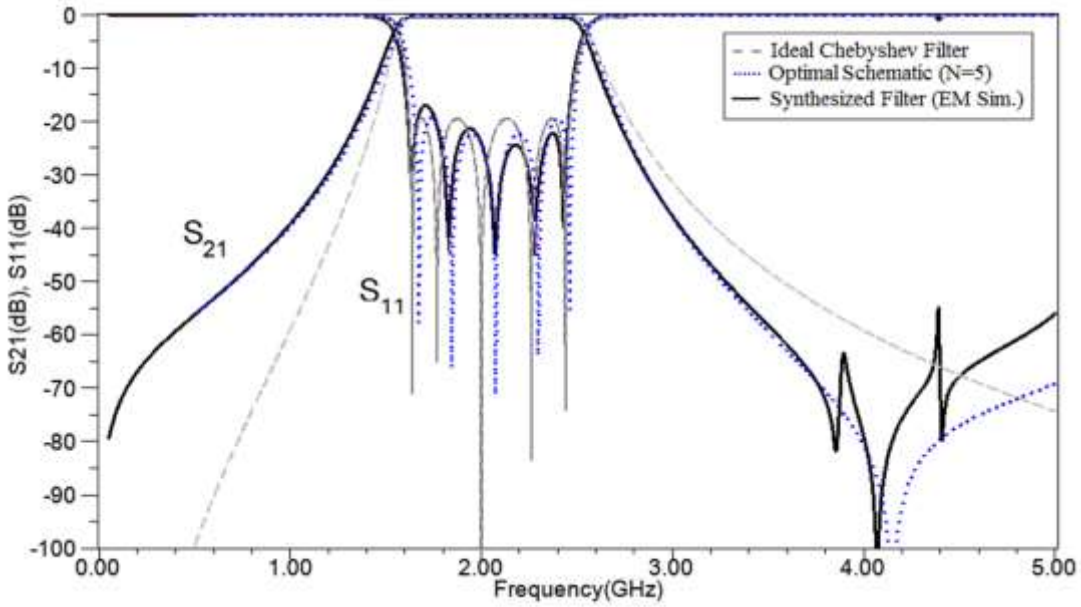

Fig 10. - Frequency response of the designed bandpass filter: EM simulation (black solid line), optimal schematic (dotted line), circuital simulation of ideal filter (grey dashed line).

In Fig. 10 we compare the simulated responses for the equivalent circuits corresponding to an ideal Chebyshev filter, our optimal schematic and the full-wave EM simulation of the designed filter. The frequency responses are rather similar, even though the level of the first lobe of the return losses ($|S_{11}|$) is above the desired value. To some extent, it can be attributed to the fact that the line sections do not have exactly 50 ohms, and to the phase shift contribution from each OCSRR resonator.

6. Conclusions

In conclusion, ASM is proved to be a powerful tool for the synthesis of wide-band filters based on OCSRRs in microstrip technology. The methodology has been validated with the complete design of 2 filter prototypes (one of order 3 and the other of order 5). The first filter example has been fabricated, and measurements agree well with the simulated data. It is relevant to comment that the proposed two-step ASM algorithm finds the layout of the complete filter, starting from the target specifications, in a completely automated way.

Acknowledgements

This work has been supported by MINECO-Spain (projects TEC2010-17512 METATRANSFER, TEC2013-47037-C5-1-R, CONSOLIDER EMET CSD2008-00066, TEC2013-40600-R and TEC2013-49221-EXP), *Generalitat de Catalunya* (project 2014SGR-157), and *Institució Catalana de Recerca i Estudis Avançats* (who has awarded Ferran Martín).

References

1. J-S. Hong, and M.J. Lancaster, *Microstrip Filters for RF/Microwave Applications*, John Wiley & Sons, 2001.

2. J. Martel, R. Marqués, F. Falcone, J. D. Baena, F. Medina, F. Martín, and M. Sorolla, "A new LC series element for compact bandpass filter design", *IEEE Microwave and Wireless Components Letters*, vol. 14, no. 5, pp. 210-212, May 2004.

3. M. Durán-Sindreu, A. Vélez, G. Sisó, P. Vélez, J. Selga, J. Bonache and F. Martín, "Recent Advances in Metamaterial Transmission Lines Based on Split Rings", *Proceedings of the IEEE*, vol. 99, no.10, pp. 1701-1710, Oct. 2011.

4. A. Rodriguez, J. Selga, M. Sans, V. E. Boria, and F. Martin, "Synthesis of open complementary split ring resonators (OCSRRs) through aggressive space mapping (ASM) and application to bandpass filters", *Proceedings of 44th European Microwave Conference (EuMC)*, pp. 323-326, 5-10 0ct. 2014.

5. J. W. Bandler, Q. Cheng, S. A. Dakroury, A. S. Mohamed, M. H. Bakr, K. Madsen, and J. Søndergaard, "Space mapping: The state of the art," *IEEE Transactions on Microwave Theory and Techniques*, vol. 52, pp. 337–361, Jan. 2004.

6. S. Koziel, Qingsha S .Cheng, and J. W. Bandler, "Space mapping," *IEEE Microwave Magazine*, vol.9, no.6, pp.105-122, December 2008.

7. M. Sans, J. Selga, A. Rodriguez, V. E. Boria, and F. Martin, "Design of Planar Wideband Bandpass Filters From Specifications Using a Two-Step Aggressive Space Mapping (ASM) Optimization Algorithm," *IEEE Transactions on Microwave Theory and Techniques*, vol. 62, pp. 3341-3350, Dec. 2014.

8. P. Vélez, J. Naqui, M. Durán-Sindreu, J. Bonache and F. Martín, "Common-mode supressed differential bandpass filter based on open complementary split ring resonators fabricated in microstrip technology without ground plane etching", Microwave and Optical Technology Letters, vol. 56, no. 4, pp. 910-916, April 2014.

9. P. Vélez, J. Naqui, M. Durán-Sindreu, J. Bonache and F. Martín, "Broadband microstrip bandpass filter based on Open Complementary Split Ring resonators", *International Journal of Antennas and Propagation*, vol. 2012, pp. 1-6, Oct. 2012.

10. J. W. Bandler, R. M. Biernacki, S. H. Chen, R. H. Hemmers and K. Madsen, "Electromagnetic optimization exploiting aggressive space mapping," IEEE Trans. Microwave Theory Tech., vol. 41, pp. 2874-2882, Dec. 1995.

11. D. M. Pozar, *Microwave Engineering*, Addison Wesley.

12. J. D. Baena, J. Bonache, F. Martin, R. M. Sillero, F. Falcone, T. Lopetegi, M. A. G. Laso, J. Garcia-Garcia, I. Gil, M. F. Portillo, and M. Sorolla, "Equivalent-circuit models for split-ring resonators and complementary split-ring resonators

coupled to planar transmission lines," *IEEE Transactions on Microwave Theory and Techniques*, vol. 53, no.4, pp.1451-1461, April 2005.